# Development and extended validation of a lumped parameter prediction model for analysing injury parameters in a vehicle crash

Gulshan Noorsumar[1], Svitlana Rogovchenko[1], Kjell G. Robbersmyr[1], Dmitry Vysochinskiy[1] and Andreas Klausen[2]

[1]Department of Engineering Sciences
University of Agder

[2]MotionTech, Norway

***Abstract*** **We present a lumped parameter model (LPM) for improving vehicle crashworthiness analysis. The novel methodology divides the event into two phases: until maximum crush and when the vehicle starts pitching forward. We built a three degrees of freedom (DOF) model for the analysis of a crash event supporting the vehicle development process. The model has been validated against the National Highway Traffic Safety Administration (NHTSA) finite element (FE) simulation of a truck and a sedan. The LPM shows good correlation with the FE test data. A parameter variation study, changing the thickness of the metal parts by 10% and 20%, is presented to improve the vehicle crash performance resulting in the reduction in pitching of the vehicle. The Simulink based simulation captures the change in the performance confirming the reliability of the model to predict event kinematics.**

## C.1 Introduction

Each year 1.23 million people are reported to die in road accidents and vehicle crashes have been among the major causes of mortality [1]. Even a larger number of people suffers from non-fatal injuries with many incurring a disability due to the injury. Production of vehicles that ensure safety for all road users including occupants is crucial to reduce the road related injuries.

Most vehicle safety regulations require crash testing at a specialized facility to determine the crashworthiness parameters. Car manufacturers conduct full vehicle or Vulnerable Road User (VRU) tests to ensure that the car design meets the regulations. Usually, crash-testing is time consuming and costly. Mathematical models are employed to represent crash dynamics, for example, in the case of a car impacting a barrier or another car. These models involve differential equations of

motion describing the deformation of the parts in the vehicle. The occupants inside the car can also be included in a mathematical model to predict injury values during a crash, models of a human present a valuable complement to other models, such as animal models and crash dummies. The vehicle front-end and side structures have been modified to improve energy absorption capability [2]. Finite Element Methods (FEM) have received impetus in vehicle crash modeling in the past decades. With improved computational speeds the models became more accurate and reliable for vehicle development. Benson et al. [3] presented the calculations of crashworthiness design laying the foundations for application of FEM in the automotive industry. However, development of FE models is time-consuming and needs CAD data which is not available during the early stages of vehicle design. Lumped parameter models (LPM) were first applied for modeling vehicle crash events in [4] where the vehicle was represented by three lumped mass components and eight resistances representing the deformable parts in the vehicle. The citeCd paper paved the way for many more studies using LPMs to represent the behaviour of a vehicle and occupants under impact. Recently, LPMs were used by Elkady et al. [2, 5] to develop a multi-DOF mathematical model to simulate a crash event with active vehicle dynamics control systems (VDCS). The model replicated a full frontal and offset impact between two vehicles comparing the performance of a baseline vehicle with a vehicle equipped with VDCS features. It also includes a 3-DOF occupant impact model derived using Lagrangian formulation. Munyazikwiye et al. [6] use a mass-spring-damper model with two lumped mass components to represent a full frontal impact with a rigid barrier. The study shows good correlation with test data suggesting that a simple LPM can replicate the impact kinematics successfully.

Occupant injury prediction is an important area of research where the vehicle-occupant interaction in a vehicle impact scenario is studied and the injury patterns of occupants in the car are determined with a help of mathematical models. Large vehicle deceleration has been identified as one of the main causes of head and chest injuries, and vehicle rotational motions in different axes also lead to occupant injuries [7].

In a full frontal impact, vehicle pitch and drop are significantly larger compared to rolling and yawing motions. Neck injury is one of the most common types of injury in vehicle accidents [8]. In a vehicle crash, unbelted occupants could interact with the vehicle interiors leading to severe injuries. In the recent past, the research focusing on unbelted occupants to meet Federal Motor Vehicle Safety Standards (FMVSS 208) requirements demonstrated that vehicle pitch and drop contributed to higher head and neck injury values.

The objective of a vehicle structure is not just to absorb energy and optimize crash pulses, but also to minimize vehicle pitch and drop [7, 9]. Chang et al. [10] have

developed an FE model to study vehicle pitch and drop in body-on-frame vehicles. The model is correlated to barrier tests and predicts factors affecting vehicle pitch and drop in a crash event. This research points to the fact that design of vehicle rails plays an important role in the load distribution during an impact scenario for body-on-frame vehicles. The out-of-plane bending of the vehicle rails increases the role of a vertical component of the barrier force, causing an imbalance in the vehicle, leading to forward pitching on the vehicle. Wei et al. [11] have estimated the relationship between energy absorbing components and the crash pulse, establishing that the bumper and the front rails both significantly contribute to the energy absorption in a full frontal crash event.

Researchers use different methodologies to improve vehicle crashworthiness modifying the vehicle structure or materials used to manufacture different vehicle parts. Genetic algorithm to estimate and optimize the vehicle parameters for a vehicle-vehicle impact was used in [12]. Li et al. [13] used lightweight optimization and material modification to meet crashworthiness requirements balancing contradictory vehicle dynamics and fuel economy requirements. The design optimization using a DOE to develop surrogate models reducing the pitch and drop in an FE model that improves interactions between the occupant's head and vehicle interior parts was presented in [14]. Our paper is an extension of the work presented by the authors at the conference SIMULTECH 2021 [15]. The model developed has been extended to validate a sedan FE model. We establish the robustness of the model to predict the impact of changes in stiffness of the vehicle on the reduction of vehicle pitching. To this end, we simplify the system splitting the vehicle motion into two phases as in [15]:

- the horizontal linear motion, and
- the rotation of the vehicle body.

We replicate a full frontal vehicle crash event at 56 kilometers per hour (kmph) employing an LPM with multiple DOFs to predict

- the maximum deformation in the vehicle to absorb energy, and
- the pitch angle of the vehicle due to the crash response.

The model has been validated with a 2014 pickup truck (Chevrolet Silverado) and a 2010 sedan (Toyota Yaris). FE model simulations of the two cars were used to compare the LPM results. The Toyota Yaris FE model has also been modified to study stiffness variations in the crashworthiness of the vehicle. The LPM is robust to predict the changes in stiffness of the vehicle making this model suitable for prediction of injury parameters in a vehicle crash.

## C.2 Methodology

Literature documents that a crash event leads to pitching, rolling and yawing of the vehicle along with the deceleration of the vehicle and movement in horizontal and vertical directions. It is difficult to model the impact scenario in different axes and to generate the governing equations. It was observed that the time for the vehicle to attain minimum velocity after impact coincides with the maximum deformation on the vehicle.

In this study, we separate the horizontal translational motion from the vertical motion during the impact event. In a full frontal crash event the vehicle experiences forward pitching; whereas the effect of rolling and yawing can be neglected. Taking into account these assumptions we split the crash event into two phases:

- time interval until maximum deformation and minimum vehicle velocity after start of crash event $t_1$, and
- time interval after maximum deformation to the end of the crash event $t_2$.

### C.2.1 FEM Simulations for Validation

We conducted a FE simulation for a 2014 Chevrolet Silverado and a 2010 Toyota Yaris running at 56 kmph and hitting a frontal barrier at 0% offset. These FE models were developed by National Crash Analysis Center (NCAC) in collaboration with NHTSA (National Highway Traffic Safety Administration) through the reverse engineering process [16].

**Chevrolet Silverado model** The FE model in Figure C.1 consisting of 1,476 parts, 2,741,848 nodes and 2,870,507 elements has been correlated to NHTSA Oblique Test and Insurance Institute for Highway Safety (IIHS) Small Overlap Front Test. The FE model weighs 2,582 kg which is close to the physical test vehicle weighing 2,624 kg. It replicates the material and geometrical properties of the physical vehicle [17].

**Toyota Yaris model** The FE model replicates a 2010 four-door passenger sedan consisting of 917 parts, 1,480,422 nodes and 1,514,068 elements. The FE model weighs 1,100 kg which is close to the physical test vehicle weighing 1,078 kg. The validation is conducted against an NCAP frontal wall impact with actual data from NHTSA Tests 5677 and 6221. It replicates the material and geometrical properties of the physical vehicle [18]. The model was also validated against test data from other scenarios. The curves correlate well with the test data and the FE model has been used by several authors [19].

The FE models were run on LS-DYNA with 32 CPUs in an HPC environment and the corresponding curves generated were used for the parameter estimation and

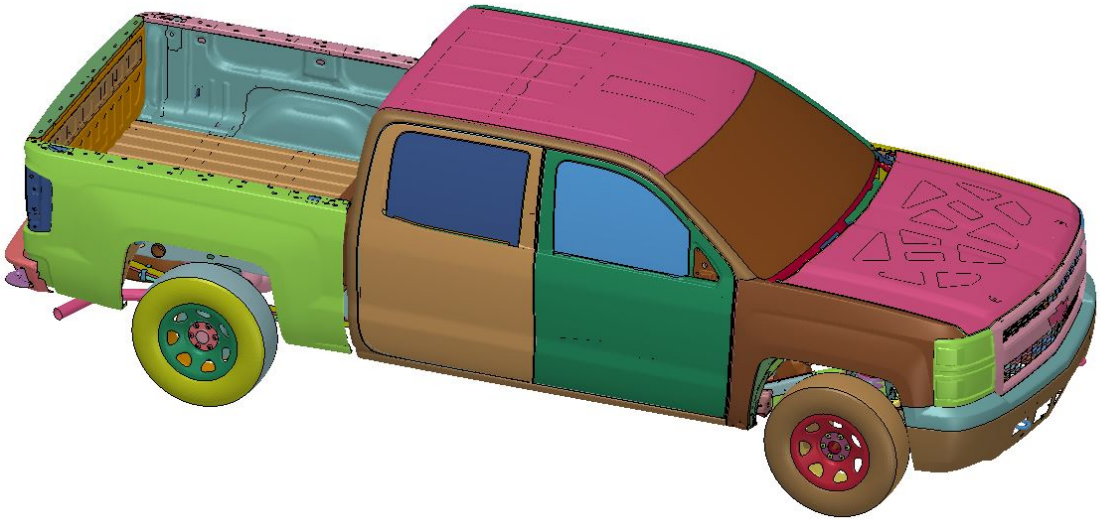

Figure C.1: An FE Model of a 2014 Chevrolet Silverado developed by NCAC [15]

validation of the LPM in MATLAB Simulink. In the FE simulation, the acceleration of some nodes on the vehicle body are recorded by the solver LS-DYNA. These nodes are selected by the user at the pre-processing stage. This process was employed to determine the acceleration of the vehicle center of gravity (CG) as well as the barrier forces, employed for the validation. Figure C.1 and C.2 shows the FE model used in the simulations. These FE model generated the piecewise linear curve data for

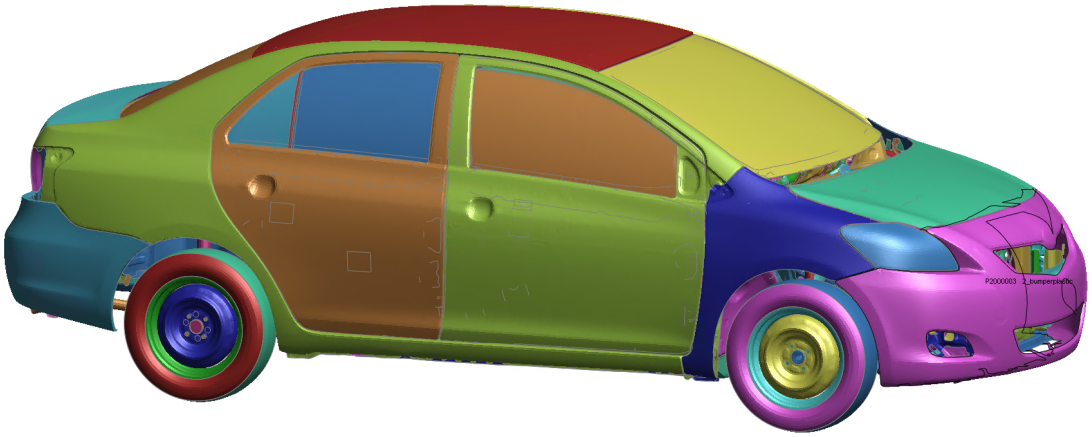

Figure C.2: An FE model of a 2010 Toyota Yaris developed by NCAC

the spring and damper coefficients. Newton-Euler numerical integration is used to calculate the values and predict the time for maximum dynamic crush of the vehicle. The algorithm is discussed in the following section.

The Toyota Yaris FE model was further updated to increase the stiffness by changing the thickness of all the metal parts by 10% and 20%. This was achieved by changing the shell element thickness on the FE regardless of the parts being load bearing or deformable members. The parts undergoing thickness change are

represented in Figure C.3. The increase in vehicle mass, mass moment of inertia and, change in vehicle CG were noted and updated in the LPM. The FE simulations were run and validated against the LPM to compare the performance.

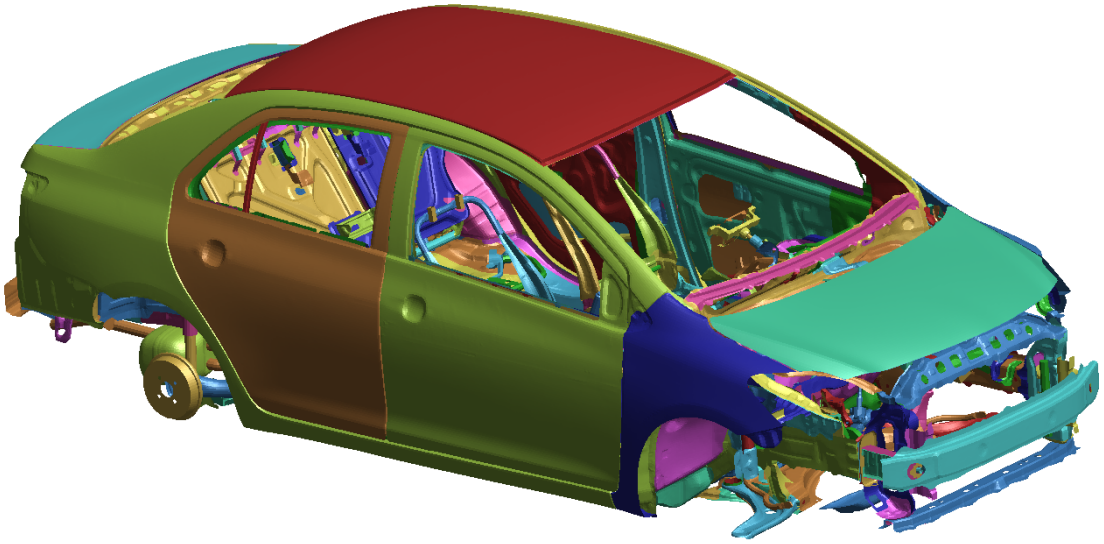

Figure C.3: Toyota Yaris metal parts undergoing thickness change for robustness study

### C.2.2 Description of the Lumped parameter model

As a single-mass system, the LPM developed utilizes a spring and damper system in the front side as the bumper and deformable system; this is commonly known as the Kelvin model. The front springs allow translational motion only in the direction of x-axis [20]. There are two pairs of springs and dampers in the suspension of the vehicle, allowing translation in the $z$ axis and rotation around the $y$-axis. There are three degrees of freedom in this system, making it quite challenging to solve. The lumped mass body can move in the direction of horizontal ($x$) and vertical ($z$) axes along with the rotation around one ($y$) axis. The CG of the vehicle is located at a distance $l_f$ from the front end and $l_r$ from the rear end suspension points; $l_0$ represents the distance between the CG and the front occupant compartment zone. The two phases are described below.

### C.2.3 Vehicle Crash Model - Phase I

First we model only the translational movement along the horizontal axis of the vehicle hitting the barrier at 0% offset. The LPM developed in Simulink replicates the maximum vehicle deformation until the time of maximum crush $t_m$. Additionally, this value corresponds to the instant the vehicle reaches its zero velocity or minimum speed. If the vehicle front end does not absorb energy by deforming plastically, then

it is possible that it will not reach zero velocity by the time of maximum deformation. A single DOF equation with a spring-damper unit is used in the mathematical model. The stiffness of the spring is tuned to represent the maximum deformation of the vehicle at a particular speed. For this problem we have assumed the speed of 56 kmph (NHTSA regulations for frontal crash). The motion of suspension system in the model has been neglected during this phase of the event. Figure C.4 represents the vehicle in a deformed state. The Simulink model predicts the time until the maximum deformation of the vehicle and the maximum displacement of the vehicle CG.

The prediction of the values of spring deformation coefficient $k$ and damper coefficient $c$ used in the general equation of motion has been a challenge for researchers in the past [21], [22]. The stiffness of the vehicle front in a crash was estimated using various parameter estimation studies. Despite the highly nonlinear behavior of the front end, it was approximated by a piecewise linear relationship [23, 24].

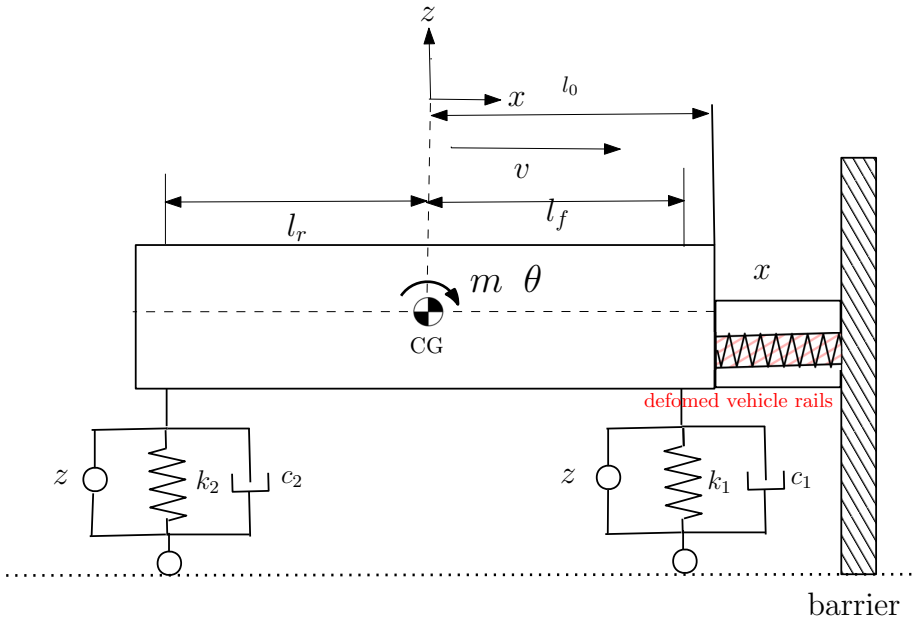


Figure C.4: Vehicle representation in Phase 1 of the event: Deformed front end [15]

In our case the equation of motion assumes the form:

$$m\ddot{x} + c\dot{x} + kx = Q_i \tag{C.1}$$

where $Q_i = 0$ (i.e. no force component is added here); $k$ is the spring coefficient; $c$ is the damper coefficient for the bumper model.

**Optimization algorithm**

At this stage, the spring and damper coefficients are parameterized using a gradient-descent optimization algorithm developed in [25] for a single mass-spring-damper system. The code searches for a global minima by performing 100 re-runs of gradient

descent optimization, each with randomly generated initial parameter values. The algorithm was modified to improve the correlation between the test and computed values. The non-linear force-deformation curve for the spring-damper system is assumed to be piecewise-linear with six breakpoints in the curve. The forces on the spring are calculated using the general relationship between the force and deformation for a spring-damper system [2], see Figure C.5. The stiffness of the spring $k$ and the spring force component $F_k$ vary according to the deflection values in the spring.

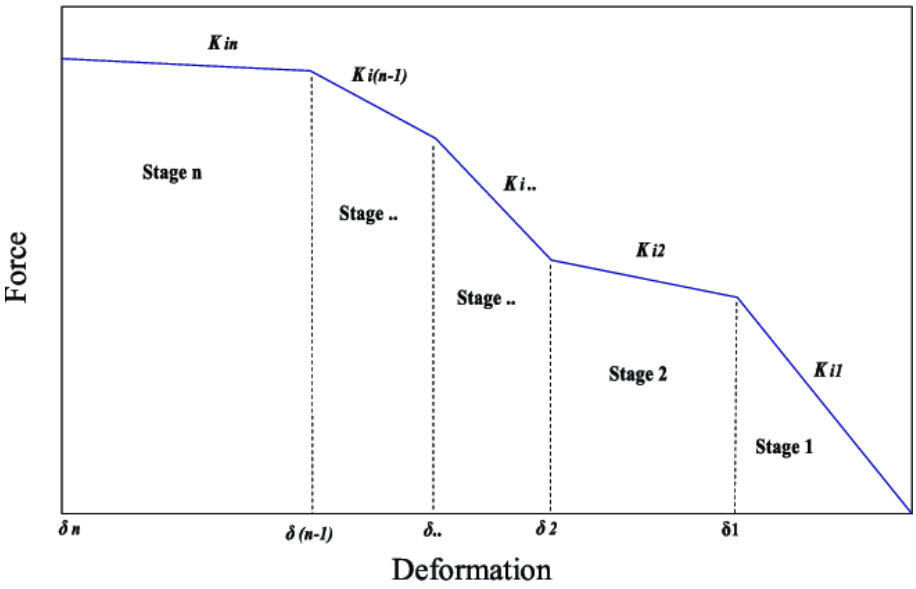


Figure C.5: General piecewise force-deformation characteristics [2], [15]

The spring stiffness and damping coefficients in the model are defined as the piecewise-linear functions of $x$ and $\dot{x}$, respectively:

$$k(x) = \begin{cases} \frac{(k_2-k_1)\cdot|\hat{x}|}{x_1} + k_1, & \text{for } |\hat{x}| \le x_1, \\ \frac{(k_3-k_2)\cdot(|\hat{x}|-x_1)}{(x_2-x_1)} + k_2, & \text{for } x_1 \le |\hat{x}| \le x_2, \\ \frac{(k_4-k_3)\cdot(|\hat{x}|-x_2)}{(x_3-x_2)} + k_3, & \text{for } x_2 \le |\hat{x}| \le x_3, \\ \frac{(k_5-k_4)\cdot(|\hat{x}|-x_3)}{(x_4-x_3)} + k_4, & \text{for } x_3 \le |\hat{x}| \le x_4, \\ \frac{(k_6-k_5)\cdot(|\hat{x}|-x_4)}{(x_5-x_4)} + k_5, & \text{for } x_4 \le |\hat{x}| \le x_5, \\ \frac{(k_7-k_6)\cdot(|\hat{x}|-x_5)}{(C-x_5)} + k_6, & \text{for } x_5 \le |\hat{x}| \le C. \end{cases}$$

The damper characteristics are defined similarly to the spring characteristics:

$$c(\dot{x}) = \begin{cases} \frac{(c_2-c_1)\cdot|\hat{\dot{x}}|}{\dot{x}_1} + c_1, & \text{for } |\hat{\dot{x}}| \leq \dot{x}_1, \\ \frac{(c_3-c_2)\cdot(|\hat{\dot{x}}|-\dot{x}_1)}{(\dot{x}_2-\dot{x}_1)} + c_2, & \text{for } \dot{x}_1 \leq |\hat{\dot{x}}| \leq \dot{x}_2, \\ \frac{(c_4-c_3)\cdot(|\hat{\dot{x}}|-\dot{x}_2)}{(\dot{x}_3-\dot{x}_2)} + c_3, & \text{for } \dot{x}_2 \leq |\hat{\dot{x}}| \leq \dot{x}_3, \\ \frac{(c_5-c_4)\cdot(|\hat{\dot{x}}|-\dot{x}_3)}{(\dot{x}_4-\dot{x}_3)} + c_4, & \text{for } \dot{x}_3 \leq |\hat{\dot{x}}| \leq \dot{x}_4, \\ \frac{(c_6-c_5)\cdot(|\hat{\dot{x}}|-\dot{x}_4)}{(\dot{x}_5-\dot{x}_4)} + c_5, & \text{for } \dot{x}_4 \leq |\hat{\dot{x}}| \leq \dot{x}_5, \\ \frac{(c_7-c_6)\cdot(|\hat{\dot{x}}|-\dot{x}_5)}{(v_0-\dot{x}_5)} + c_6, & \text{for } \dot{x}_5 \leq |\hat{\dot{x}}| \leq v_0, \end{cases}$$

where $k$ is the spring coefficient, $c$ is the damper coefficient, $\hat{x}$ is the computed vehicle deformation, $\dot{x}$ is the vehicle velocity, $\hat{\dot{x}}$ is the computed vehicle velocity, $v_0$ is the velocity at the time of maximum dynamic crush, C is the maximum dynamic crush, $F_k$ and $F_c$ are the built-up spring and damping forces defined by the following equations

$$F_k = k(x) \cdot x, \tag{C.2}$$

$$F_c = c(\dot{x}) \cdot \dot{x}. \tag{C.3}$$

The proposed algorithm uses an optimization approach to minimize an objective function. The objective function to be minimized is the error function $E(\Theta, t)$ where $\Theta$ denotes the unknown variables in the mode. The error function is defined as follows: $E(\Theta, t) = E_1(\Theta, t) + E_2(\Theta, t) + E_3(\Theta, t)$ where

$$E_1(\Theta, t) = |(a_{FE} - a_{LPM})|, \tag{C.4a}$$

$$E_2(\Theta, t) = |(v_{FE} - v_{LPM})|, \tag{C.4b}$$

$$E_3(\Theta, t) = |(x_{FE} - x_{LPM})|, \tag{C.4c}$$

where $a$ is the acceleration, $v$ is the vehicle velocity, and $x$ is the displacement. The error function $E(\Theta, t)$ determines the difference between the FE values and LPM values at every point, and the optimization algorithm minimizes the error values by altering $\Theta = [k_i, c_i], \quad \forall i \in [1, 7]$. The corresponding spring and damper coefficient values obtained from this minimization algorithm are discussed in the results section.

### C.2.4 Vehicle Crash Model - Phase II

The second phase for the model describes what happens after the instant the vehicle achieves maximum dynamic crush and minimum velocity. At this instant the vehicle starts to pitch forward. Several studies were conducted to understand the vehicle pitching forward [7, 26] suggesting that for the body-on-frame vehicles one of the reasons is the out-of-plane bending in vehicle rails which leads to the appearance of a vertical force component in the moment balance equation. This vertical force component is added to gravity force acting downwards and creates an imbalance of loading resulting in the vehicle pitching. The prediction of the pitching angle is important for determining the injury to occupants. Low pitching angles influences occupant protection design in a vehicle. This phase of the event is shown in Figure C.6 and Figure C.7. We consider here only vertical motion of the suspension springs and the rotation about the $y$-axis with angle $\theta$.

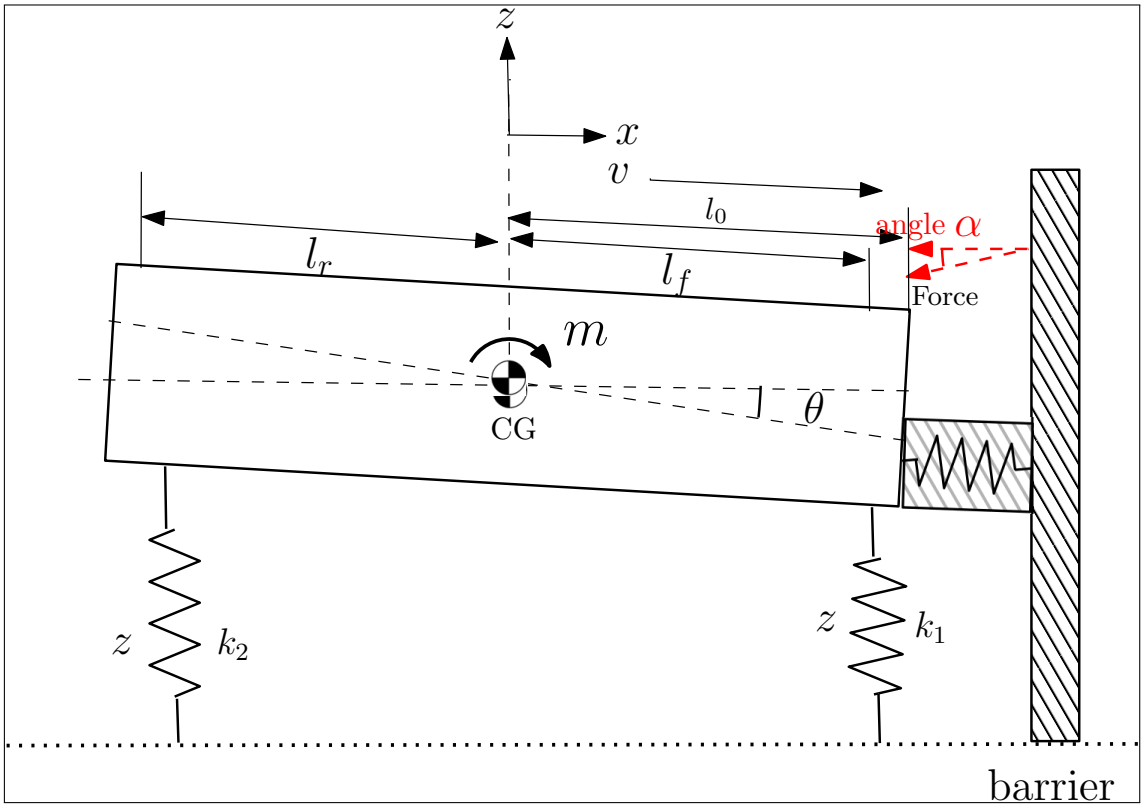


Figure C.6: Vehicle representation in Phase II of the event: Vehicle Pitching forward [15]

The dynamics in the Lagrangian formulation is described by the equation [27]:

$$\frac{d}{dt}\frac{\partial L}{\partial \dot{q}_i} - \frac{\partial L}{\partial q_i} + \frac{\partial D}{\partial q_i} = Q_i \tag{C.5}$$

where, in the general case, $L = T - V$, $T$ is the total kinetic energy of the system

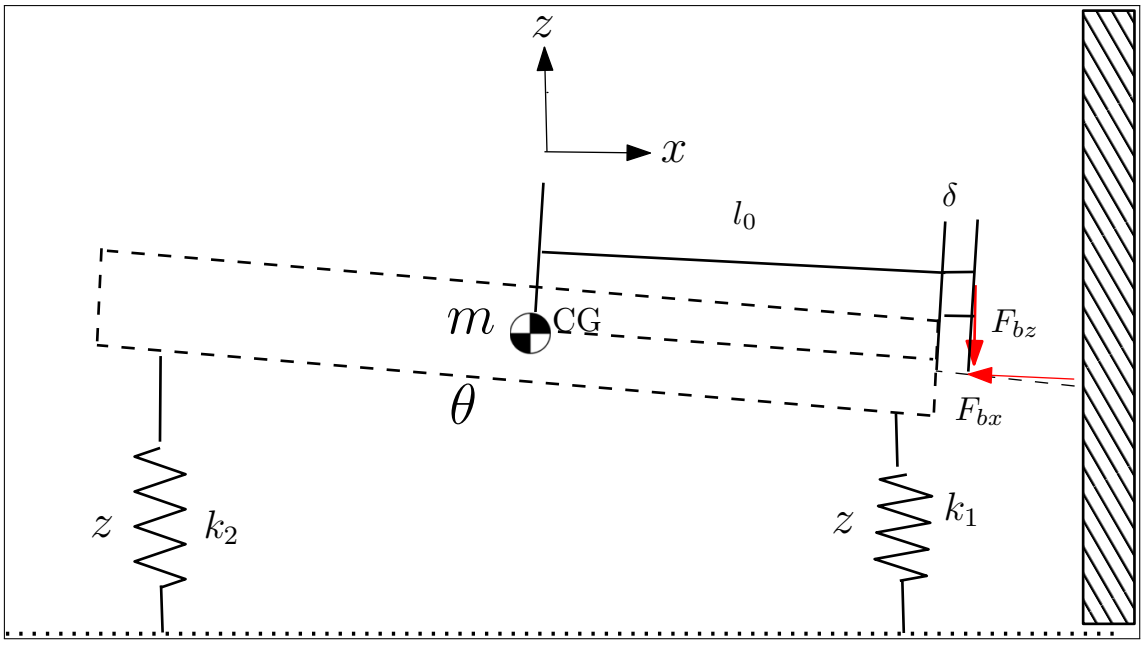


Figure C.7: Vehicle representation in Phase II with forces acting on the vehicle and suspension springs in play [15]

equal to the sum of the kinetic energies of the particles, $q_i\, i = 1, \ldots, n$ are generalized coordinates, $Q_i$ is the external force acting on the system, which in this case is the vertical force component experienced by the vehicle at the time of maximum dynamic crush, and $V$ is the potential energy of the system. For dissipation forces, a special function $D$ must be introduced alongside $L$.

The equations for the kinetic, potential and dissipation energy are:

$$T = \frac{1}{2}J\dot{\theta}^2 + \frac{1}{2}m\dot{x}^2, \tag{C.6}$$

$$V = \frac{1}{2}k_1(x - l_f\theta)^2 + \frac{1}{2}k_2(x + l_r\theta)^2, \tag{C.7}$$

and

$$D = \frac{1}{2}c_1(\dot{x} - l_f\dot{\theta})^2 + \frac{1}{2}c_2(\dot{x} + l_r\dot{\theta})^2. \tag{C.8}$$

The values of standard automotive parameters $k_1$, $k_2$, $c_1$, $c_2$, $l_f$ and $l_r$ are taken from the literature, [28], see Table C.1.

Table C.1: Automotive Parameters set [28]

| Symbol | Value | Unit | Meaning |
|---|---|---|---|
| $M$ | 400 | kg | Sprung mass |
| $m_{ij}$ | 50 | kg | Unsprung masses ($i$ = front, rear and $j$ = left, right) |
| $I_x$ | 250 | kg.m$^2$ | Roll inertia |
| $I_y$ | 1400 | kg.m$^2$ | Pitch inertia |
| $t$ | 1.4 | m | Front and rear axle |
| $l_f$ | 1.4 | m | COG-front distance |
| $l_r$ | 1 | m | COG-rear distance |
| $r$ | 0.3 | m | Nominal wheel radius |
| $h$ | 0.7 | m | Chassis COG height |
| $k_f$ | 30,000 | N/m | Front suspension linearized stiffness (left, right) |
| $k_r$ | 20,000 | N/m | Rear suspension linearized stiffness (left, right) |
| $c_f$ | 1500 | N/m/s | Front suspension linearized damping (left, right) |
| $c_r$ | 3000 | N/m/s | Rear suspension linearized damping (left, right) |
| $k_t$ | 200,000 | N/m | Tire stiffness (front, rear and left, right) |
| $\beta$ | 50 | rad/s | Suspension actuator bandwidth |

The values of the vehicle mass $m$ and the moment of inertia $J$ for the lumped mass system are calculated from the FE model of the vehicle. The governing equations of motion are [15]:

$$\begin{aligned} Q_i =& J\ddot{\theta} + (k_1 l_f^2 + k_2 l_r^2)\theta + (c_1 l_f^2 + c_2 l_r^2)\dot{\theta} \\ &+ (k_2 l_r - k_1 l_f)x + (c_2 l_r - c_1 l_f)\dot{x}, \end{aligned} \tag{C.9}$$

$$\begin{aligned} Q_i =& m\ddot{x} + (k_1 + k_2)x + (c_1 l_f + c_2 l_r)\dot{\theta} \\ &+ (k_2 l_r - k_1 l_f)\theta + (c_1 + c_2)\dot{x}. \end{aligned} \tag{C.10}$$

### C.2.5 Robustness Check

The LPM predicts important vehicle parameters, thus, contributing to analysis of vehicle crashworthiness. The model was validated to estimate the injury parameters for a truck and a sedan. The sensitivity of the model to stiffness is assessed by changing the thickness of the material; analyzing the spring and damper coefficient curves generated with the help of the optimization algorithm described in Section C.2.3. The methodology for determining the vehicle parameters (maximum displacement, time for zero velocity and maximum pitch angle) is similar to the baseline model. It is interesting to observe the changes in vehicle pitching angle and acceleration by adding mass to the system in terms of elemental thickness to the metal parts.

The changes in mass and moment of inertia for the model are presented in Table C.2 below. These changes have been incorporated in the LPM to determine injury values.

Table C.2: FE Model specifications

| Parameter | Yaris Baseline | 10% stiffness | 20% stiffness |
|---|---|---|---|
| Mass, (kg) | 1253.5 | 1303.9 | 1353.6 |
| Mass Moment of Inertia, ($kgm^2$) ($I_{xx}$) | 425128 | 445472 | 465782 |
| Vehicle CG $x$, (mm) | 1025 | 1033.6 | 1039 |
| Vehicle CG $y$, (mm) | -3.0 | -2.1 | -1.5 |
| Vehicle CG $z$, (mm) | 557 | 560 | 563 [1ex] |

## C.3 Results and Discussion

In this section we compare the results of the LPM with FE data generated from LS-DYNA simulations for a Chevrolet Silverado and Toyota Yaris vehicle at 56 kmph with a full frontal impact loadcase.

### C.3.1 Phase I

**Baseline Chevrolet Silverado Model** First we simulate the time until maximum deformation of the vehicle; the spring and damper coefficients are determined using the Gradient Descent Optimization with an error function defined in Section C.2.3. The computed and test (FE) values are plotted in Figure C.8; They show good correlation of results. The predicted values of the stiffness and damping coefficients are shown in Figures C.9 and C.10.

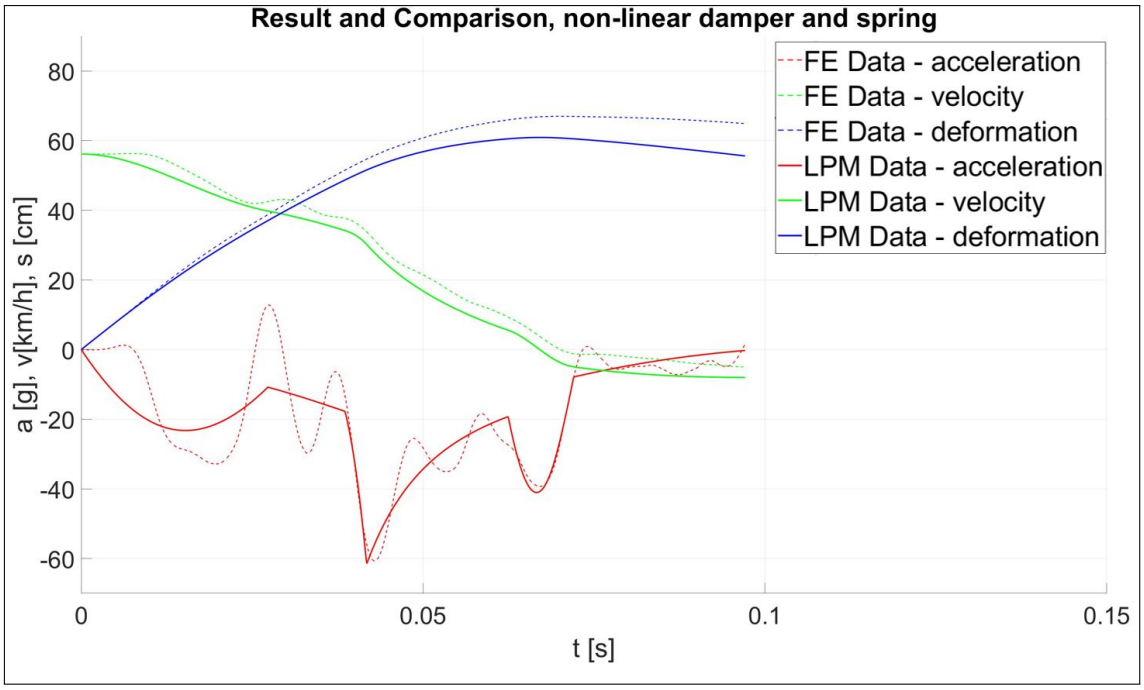


Figure C.8: Plot of computed and test values for parameter model for a Chevrolet Silverado Model

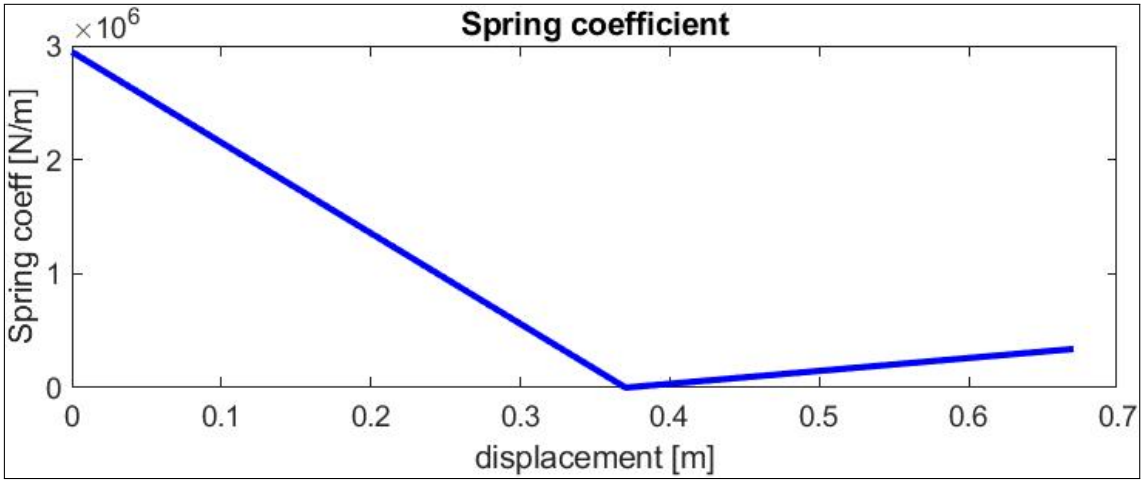


Figure C.9: Spring coefficient obtained from the algorithm for Chevrolet Silverado Baseline model

The output from the Gradient Descent Optimization algorithm is used to predict the deformation and vehicle velocity in a MATLAB Simulink model.

The plots of maximum FE vehicle deformation and LPM deformation in Figure C.11(**a**) show good correlation. A similar plot (Figure C.11(**b**)) was generated to compare the velocity of the vehicle at the CG; in the case of LPM at the lumped mass center. The LPM is represented by the mathematical model in the plots. The time the vehicle attains zero velocity is closely correlated in the plots but there is a small deviation after 40 ms. The reason for this deviation can be attributed to

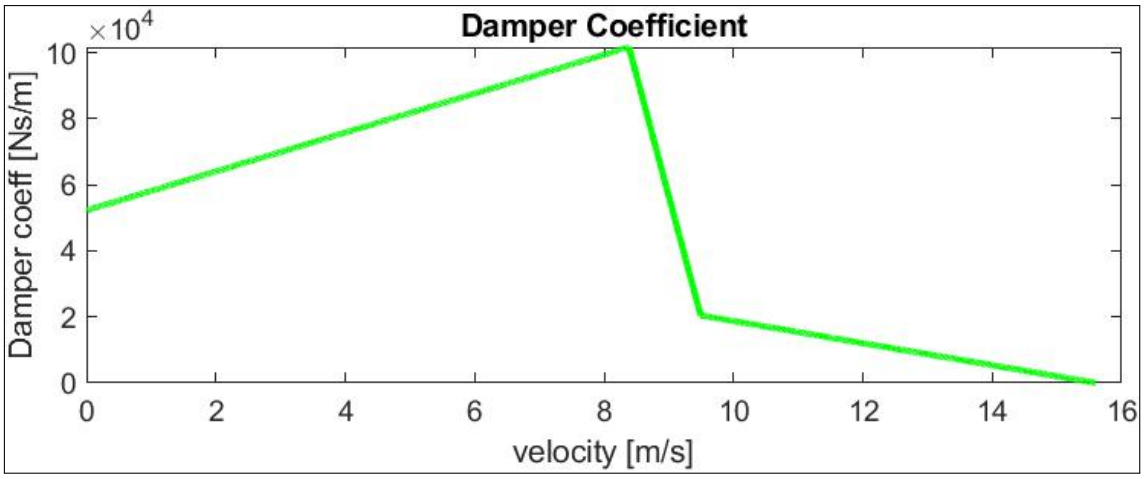


Figure C.10: Damper Coefficient obtained from the algorithm for Chevrolet Silverado Baseline model

the spring and damper characteristics which are approximated in this study using a piece-wise linear function. The model can be improved using a non-linear function for the spring stiffness and damping characteristics. If the model is simulated beyond the time the vehicle attains zero velocity, a rebound is observed in the velocity. This velocity rebound could be due to the internal strain energy stored in the springs, and it would be interesting to investigate this further in the future.

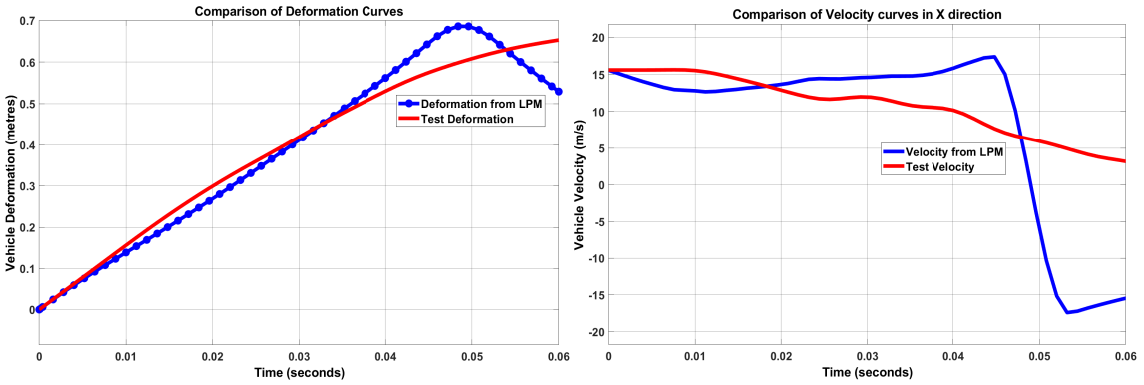


(**a**) (**b**)

Figure C.11: (a) Displacement of the vehicle CG curves comparison for LPM vs FE model, (b) velocity of the vehicle CG curves comparison for LPM vs FE model Chevrolet Silverado Baseline model - Phase I

**Baseline Toyota Yaris Model** The baseline 2010 Yaris model FE simulations were used for estimating the front-end spring-damper characteristics shown in Figure C.13; acceleration, velocity and deformation plots are compared in C.12. These characteristics are used in Phase I of the Simulink model to determine the displacement and time for the vehicle to attain zero velocity. The curves are overlayed in Figure C.14.

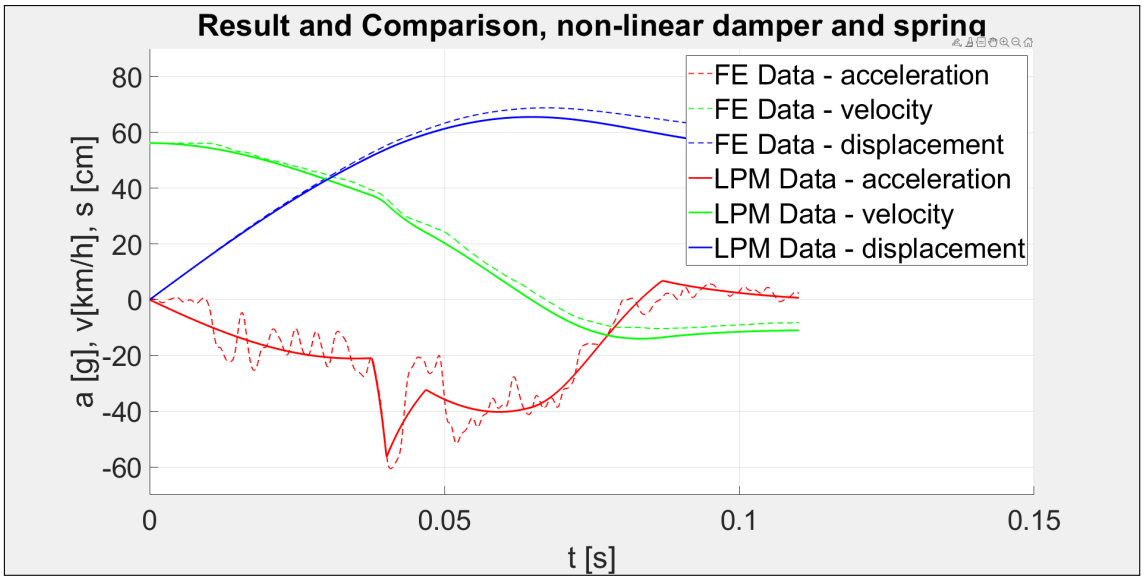


Figure C.12: Plot of computed and FE test values for lumped parameter model for a Toyota Yaris Model

## C.3.2 Phase II

The prediction for the second part of the lumped model using Simulink was conducted and plotted against the data from FE model. The quantity $Q_i$ in the governing equations is the vertical component of the barrier force experienced by the vehicle in the crash. The force curve is derived from the FE model and inputted into the Simulink model to improve the prediction; it will be of interest to mathematically explain this force component in terms of residual impact energy after absorption. The Simulink model is run with numerical integration (variable timestep- ode 45) and the velocity of the lumped mass in $z$-direction along with the pitching angle is compared to the data from FE model.

### C.3.2.1 Baseline Chevrolet Silverado Model

Figure C.15(**a**) compares the $z$-velocity (vertical velocity) in the body with the curves generated from the FE data. The trend in the curve is similar but the peak values are not matching. One of the contributing factors to this deviation is the use of standard linear spring and damper coefficient values for the model. The use of the linear approximation for the spring and damper coefficients can lead to the difference in the values for this parameter as well. The values of $l_f$ and $l_r$ can also be further tuned to represent the Chevrolet Silverado (2014) model. However, we intentionally avoided fine tuning these values assuming that this data may not be available to vehicle development team at the start of the design process and it makes sense to use

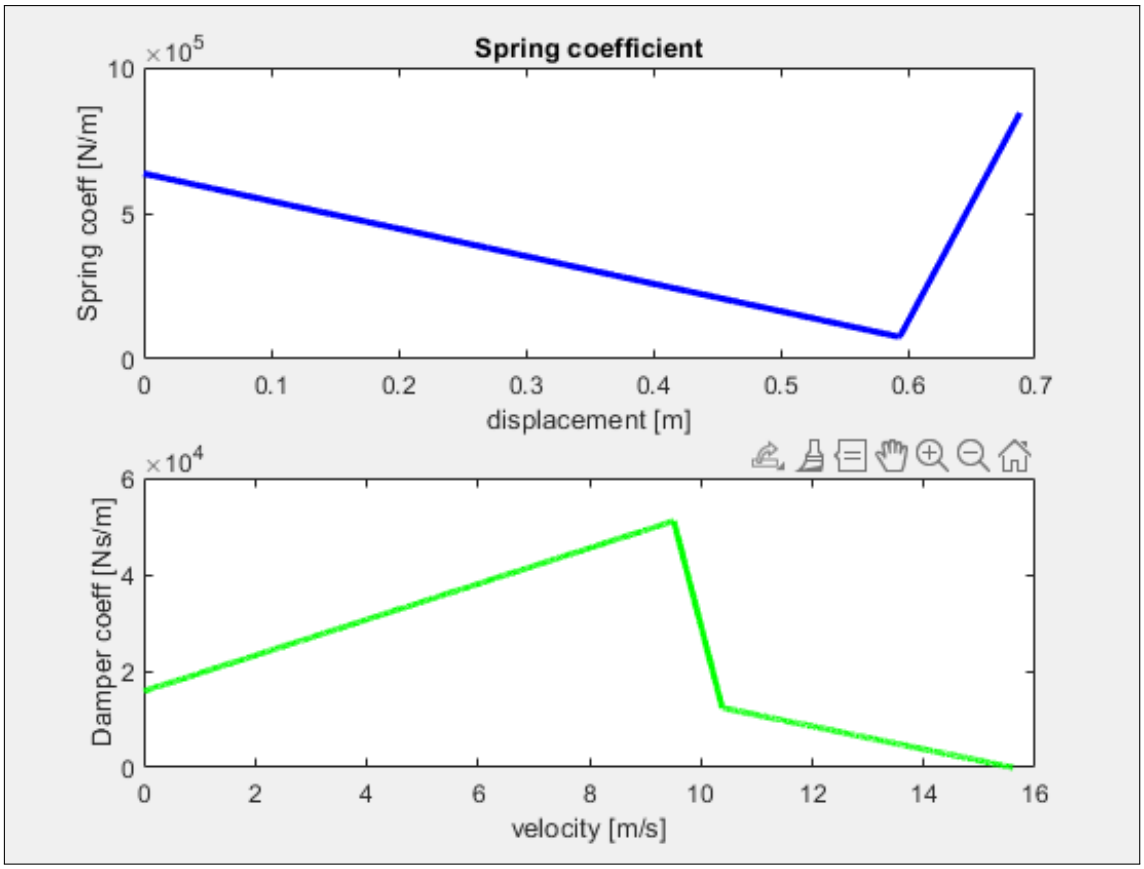


Figure C.13: Damper Coefficient obtained from the algorithm for Toyota Yaris Baseline model

standard values for automotive parameters. Figure C.15(**b**) compares the forward pitching angle for the FE model and the LPM developed in this study. The pitch angle comparison shows a similar trend observed in both curves. The vehicle starts to pitch around the same time during the crash event; this is crucial for designers planning airbag deployment in vehicles and other active protection features. The pitch angle curve for the simulation LPM peaks higher than the FE data at the start of the vehicle rotation but slowly follows the FE data curve showing comparable maximum pitch angle values. In addition, this is also a very important observation for vehicle safety designers. The difference between the curves can be explained by the linear approximation for the spring and damper coefficients and the barrier force definition. The study did not account for energy losses that may exist in the model.

#### C.3.2.2 Baseline Toyota Yaris Model

Similar to Phase I, the $z$ velocity and pitch of the vehicle is overlaid for the Yaris model in Phase II of the impact presented in Fig C.16. The observations for the prediction of the injury parameters are consistent with the truck model prompting the reliability of the model for different vehicle platforms.

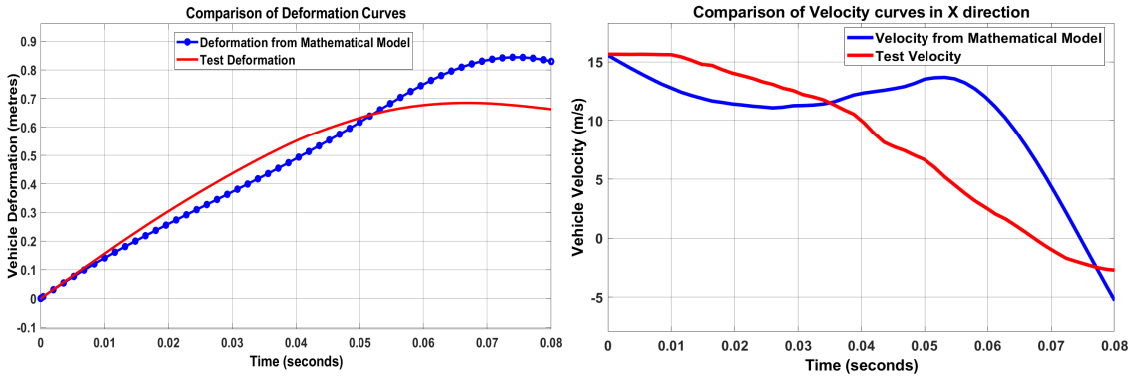


(a) (b)

Figure C.14: (a)Displacement curves overlaid, (b) Velocity curves overlaid
Toyota Yaris Baseline model Phase I : Overlay of curves for LPM and FEM

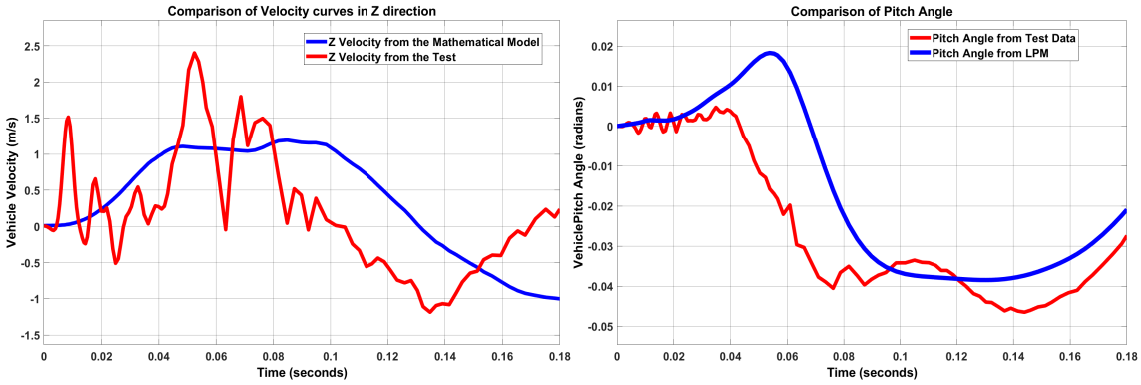


(a) (b)

Figure C.15: (a) Z-Velocity curve overlay for LPM vs FE model, (b) Forward Pitch Angle curve overlay for LPM vs FE model
Chevrolet Silverado Baseline Model Phase II : Overlay of curves for LPM and FEM

### C.3.3 Robustness Check

According to Section C.2.5 the LPM was used to predict stiffness changes in the model by changing the thickness of the model by

- increasing thickness of all metal parts by 10%
- increasing thickness of all metal parts by 20%

Figure C.17 shows the acceleration and pitch curves for the baseline Toyota Yaris model and the modified models. It is observed that increasing the thickness of the parts reduces the peak acceleration values along with the vehicle pitching forward. However, the trend is non-linear indicating that only increasing the thickness is not a possible countermeasure to improve vehicle crashworthiness. There are other contributing variables which could help reduce the injury values in a crash.

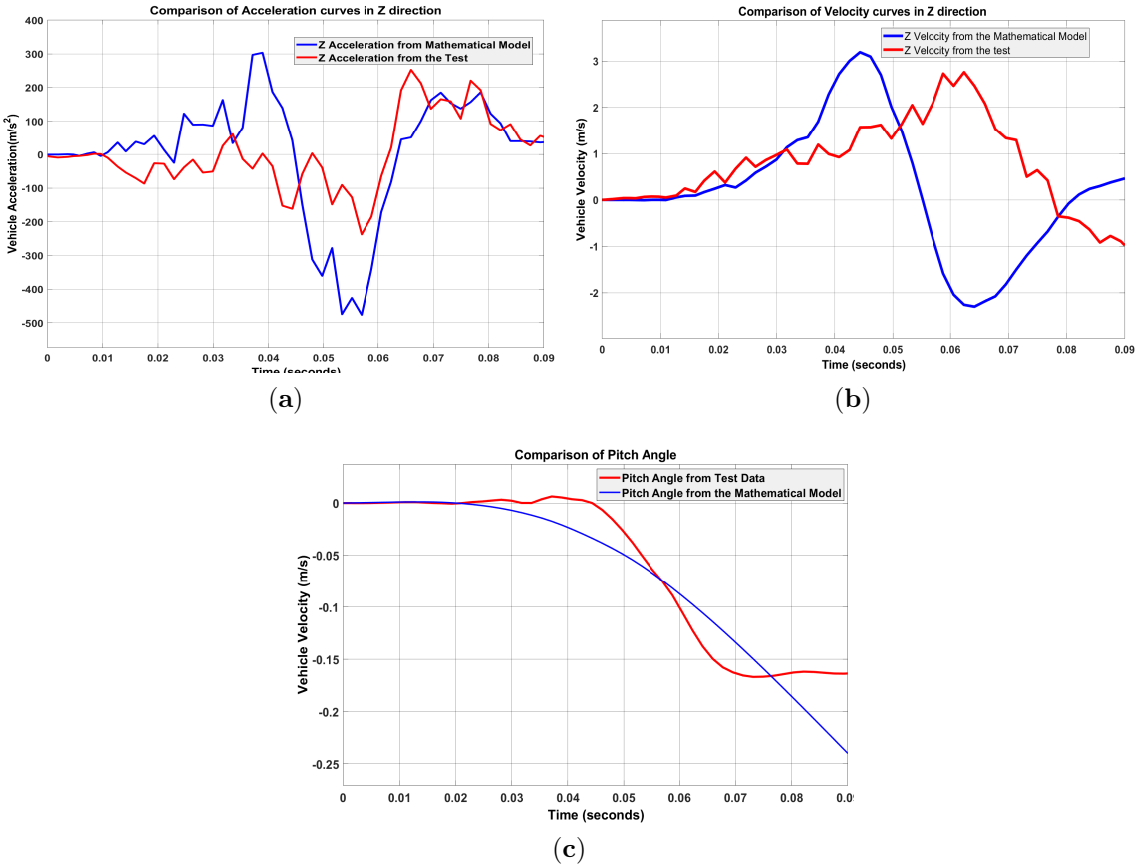


Figure C.16: (a)$Z$ Acceleration curve, (b) $Z$ Velocity curve, (c)Pitch curve Toyota Yaris Baseline Phase II : Overlay of curves for LPM and FEM

### C.3.3.1 Phase I - 10% thickness

The spring and damper coefficient curves; mass/moment of inertia changes are updated in the Simulink model to determine the performance of the LPM in both phases of impact. The maximum displacement is closely correlated to the test data in Figure C.18(**a**) and the time the vehicle attains zero velocity is predicted with a variation of approximately 10 ms.

### C.3.3.2 Phase II - 10% thickness

The simulation was repeated for the 10% stiffness model using Simulink to simulate the impact kinematics and predict the front-end deformation to absorb the energy of the impact; along with the forward pitching of the vehicle. The model predicts the maximum pitching angle and the $z$ acceleration curve is closely replicated in the LPM simulations, see Figure C.20.

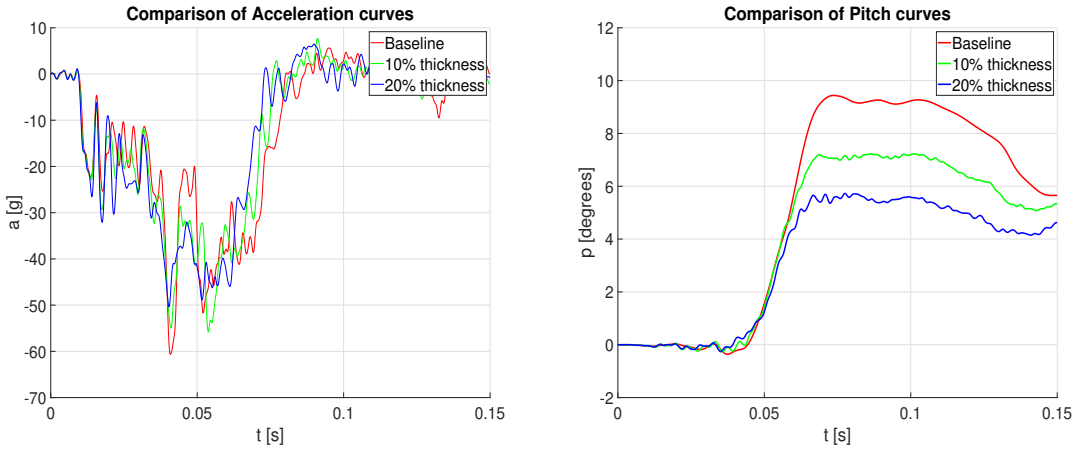


(a) (b)

Figure C.17: (a) $X$-acceleration comparison for baseline and modified models, (b) Forward Pitch Angle comparison for baseline and modified models
Toyota Yaris Model: Stiffness Variation

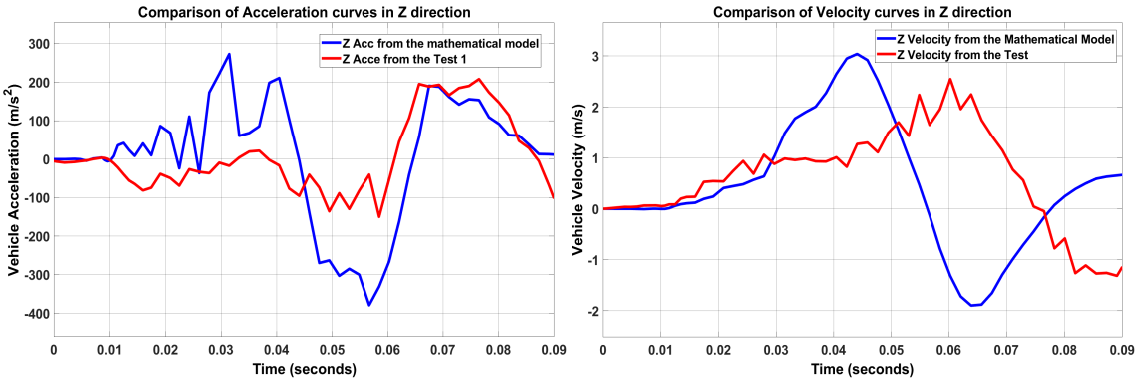


(a) (b)

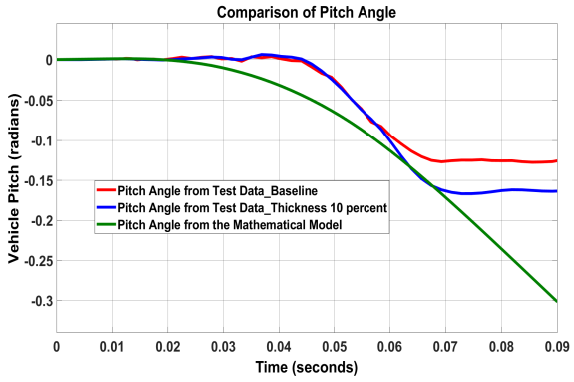


(c)

Figure C.19: (a) $Z$ Acceleration curves overlaid, (b) $Z$ Velocity curves overlaid, (c) Forward Pitching curves overlaid
Toyota Yaris Model - 10% Thickness Variation - Phase II : Overlay of curves for LPM and FEM

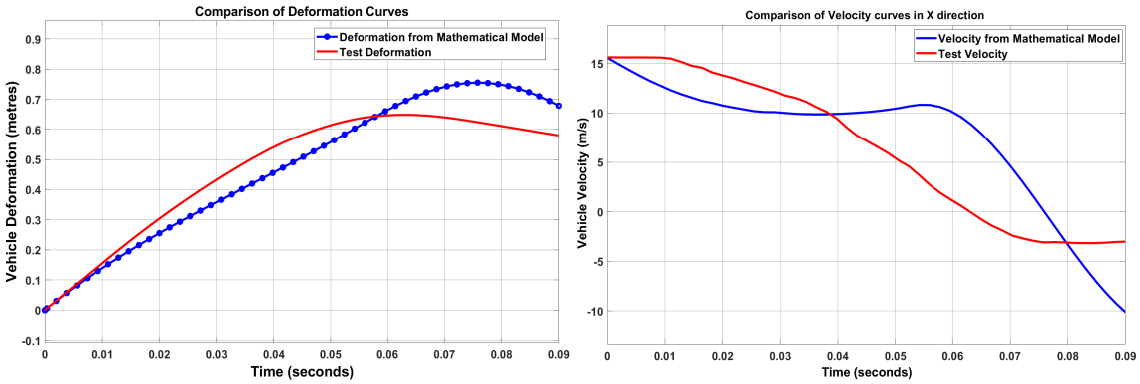


(**a**) (**b**)

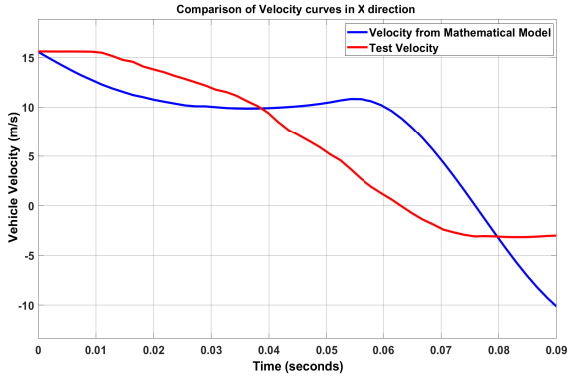


(**c**)

Figure C.18: (a)Deformation curves overlaid, (b) Velocity curves overlaid, (c) Pitch curve
Toyota Yaris Model - 10% Thickness Variation - Phase I : Overlay of curves for LPM and FEM

.

### C.3.3.3 Phase I - 20% thickness

The results of Phase I with thickness modification are presented in Figure C.20 and show good correlation with the results. The gap in correlation is consistent with the observations outlined with the Silverado model.

### C.3.3.4 Phase II - 20% thickness

The pitching curve in Figure C.21(**c**) follows the trend of the FE test data, however, the LPM simulation deviates from the test curve after the time of maximum pitching. This can be attributed to the constant stiffness of the suspension springs and damper coefficients. The LPM can be further improved by providing non-linear stiffness and damper characteristics representing the vehicle suspension system.

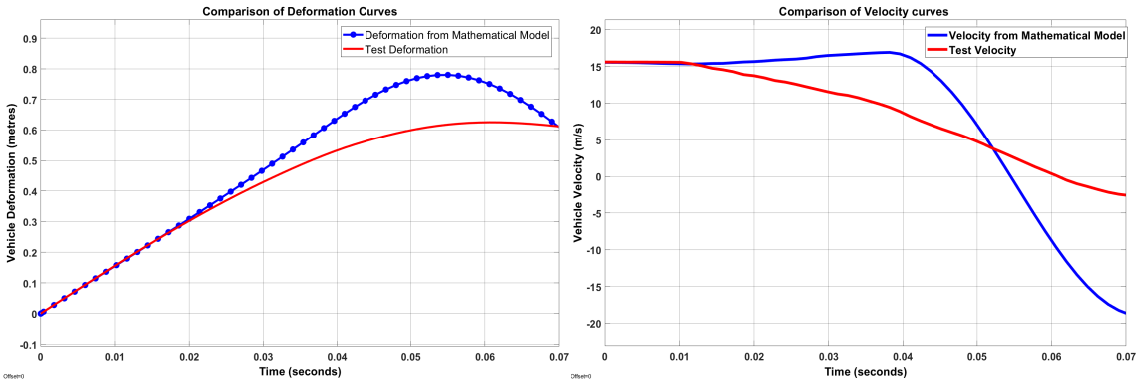


(**a**) (**b**)

Figure C.20: (a)Deformation curves overlaid, (b) $X$ velocity curves overlaid
Toyota Yaris Model - 20% Thickness Variation Phase I : Overlay of curves for LPM and FEM

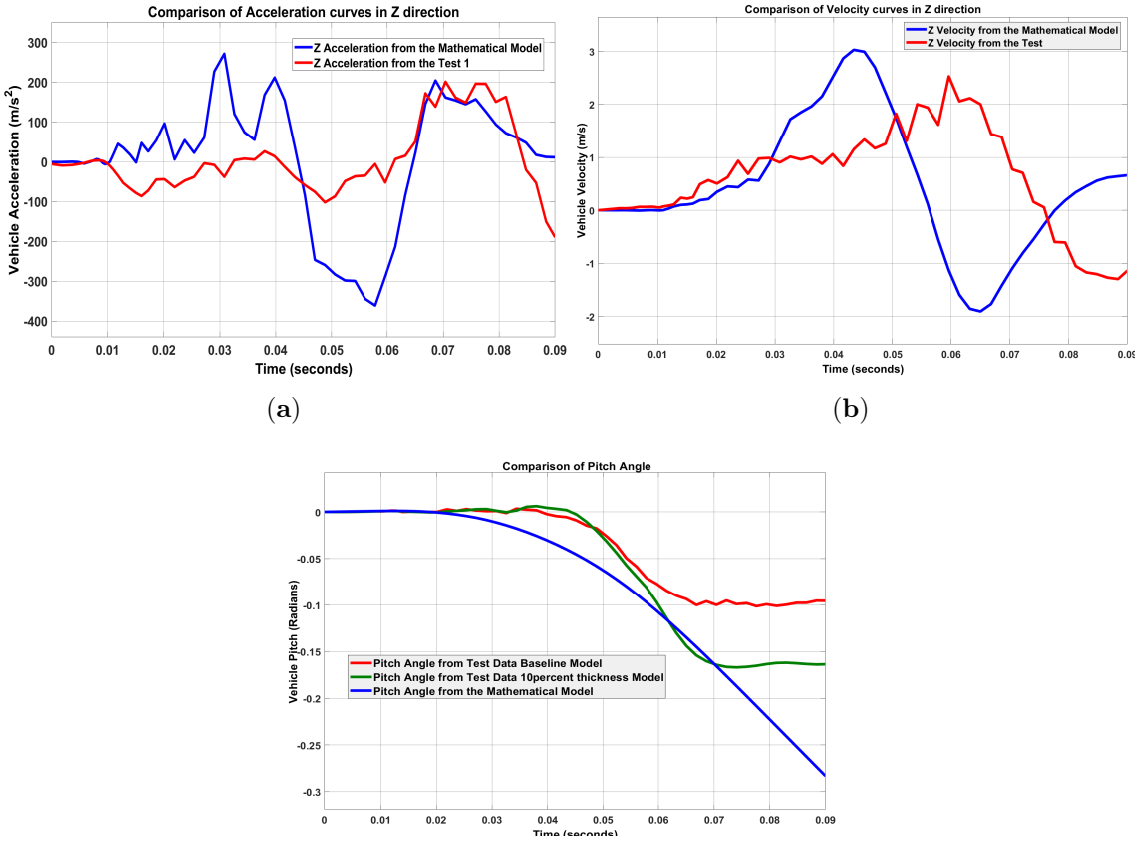


(**a**) (**b**)

(**c**)

Figure C.21: (a)$z$ Acceleration curves overlaid, (b) $z$ Velocity curves overlaid, (c) Forward Pitch curves overlaid
Toyota Yaris Model - 20% Thickness Variation - Phase II : Overlay of curves for LPM and FEM

The change in stiffness is closely predicted in both models for the $z$ acceleration and maximum pitching angle indicating a high reliability of the model. The maximum

deformation and time to attain zero velocity is also correlated well in the LPM simulations; the differences in the result can be attributed to the assumption of linear characteristics for non-linear front-end spring data.

## C.4 Conclusions

The novel technique developed in this paper for modeling a full frontal vehicle crash event successfully predicts the event kinematics. The study demonstrates that the two phase simulation model can describe a highly complex dynamical multiple DOF system with few equations and parameters, making the process of using LPMs very simple and reliable for safety design engineers. The robustness check and stiffness variation analysis indicates that the model is reliable and predicts variations in the parameters to determine injury values. The increase in thickness of the model by 10% and 20% improved the crashworthiness of the vehicle. Reducing the pitching angle would reduce the likelihood of injury to the occupants. The study highlights that parameter identification is an important part of the accident reconstruction process and influences the crashworthiness performance of the vehicle.

The assumptions used to arrive at a simpler LPM model providing reliable results include the following:

- The spring and damper characteristics are assumed to be piecewise-linear with six breakpoints although they are non-linear in physical systems.
- The suspension spring and damper coefficients were assumed same for the truck and sedan model used in the validation study.
- The vehicle acceleration is assumed to be zero at the time pitching starts in the crash event.
- Energy losses like friction and heat losses in the vehicle during the crash event are neglected to simplify the problem.
- Only vehicle rotations about the $y$-axis (pitching) are considered for modeling in the full frontal impact scenario; rotations about other axes are considered negligible and not impacting the occupant injuries.

# References – Paper C


[1] Paul Du Bois, Clifford C Chou, Bahig B Fileta, Tawfik B Khalil, Albert I King, Hikmat F Mahmood, Harold J Mertz, Jac Wismans, Priya Prasad, and Jamel E Belwafa. Vehicle crashworthiness and occupant protection. 2004.

[2] Mustafa Elkady and Ahmed Elmarakbi. Modelling and analysis of vehicle crash system integrated with different vdcs under high speed impacts. *Open Engineering*, 2(4):585–602, 2012.

[3] DJ Benson, JO Hallquist, M Igarashi, K Shimomaki, and M Mizuno. Application of dyna3d in large scale crashworthiness calculations. Technical report, Lawrence Livermore National Lab., 1986.

[4] Mounir M Kamal. Analysis and simulation of vehicle to barrier impact. *SAE Transactions*, pages 1498–1503, 1970.

[5] Mustafa Elkady, Ahmed Elmarakbi, and John MacIntyre. Enhancement of vehicle safety and improving vehicle yaw behaviour due to offset collisions using vehicle dynamics. *International journal of vehicle safety*, 6(2):110–133, 2012.

[6] Bernard B Munyazikwiye, Hamid R Karimi, and Kjell Gunnar Robbersmyr. Mathematical modeling of vehicle frontal crash by a double spring-mass-damper model. In *2013 XXIV International Conference on Information, Communication and Automation Technologies (ICAT)*, pages 1–6. IEEE, 2013.

[7] J Michael Chang, Mohammad Ali, Ryan Craig, Tau Tyan, Marwan El-Bkaily, and James Cheng. Important modeling practices in cae simulation for vehicle pitch and drop. *SAE Transactions*, pages 62–72, 2006.

[8] Fan Li, Nian Song Liu, Hong Geng Li, Biao Zhang, Shi Wei Tian, Ming Gang Tan, and Baptiste Sandoz. A review of neck injury and protection in vehicle accidents. *Transportation Safety and Environment*, 1(2):89–105, 11 2019. ISSN 26314428. doi: 10.1093/TSE/TDZ012. URL `https://academic.oup.com/tse/article/1/2/89/5618803`.

[9] Gernot Woitsch and Wolfgang Sinz. Influence of pitching and yawing during frontal passenger vehicle crash tests on driver occupant's kinematics and injury. *International journal of crashworthiness*, 18(4):356–370, 2013.

[10] J Michael Chang, Mohammed Rahman, Mohammad Ali, Tau Tyan, Marwan El-Bkaily, and James Cheng. Modeling and design for vehicle pitch and drop of body-on-frame vehicles. *SAE transactions*, pages 329–338, 2005.

[11] Zuolong Wei, Hamid Reza Karimi, and Kjell Gunnar Robbersmyr. Analysis of the relationship between energy absorbing components and vehicle crash response. Technical report, SAE Technical Paper, 2016.

[12] Bernard B. Munyazikwiye, Hamid Reza Karimi, and Kjell G. Robbersmyr. Optimization of vehicle-to-vehicle frontal crash model based on measured data using genetic algorithm. *IEEE Access*, 5:3131–3138, 2017. ISSN 21693536. doi: 10.1109/ACCESS.2017.2671357.

[13] Zhaokai Li, Qiang Yu, Xuan Zhao, Man Yu, Peilong Shi, and Cilei Yan. Crashworthiness and lightweight optimization to applied multiple materials and foam-filled front end structure of auto-body:. *http://dx.doi.org/10.1177/1687814017702806*, 9(8):1–21, 8 2017. ISSN 16878140. doi: 10.1177/1687814017702806. URL `https://journals.sagepub.com/doi/full/10.1177/1687814017702806`.

[14] J. Michael Chang, Miinshiou Huang, Tau Tyan, G. Li, and L. Gu. Structural optimization for vehicle pitch and drop. In *SAE Technical Papers*. SAE International, 4 2006. doi: 10.4271/2006-01-0316. URL `https://www.sae.org/publications/technical-papers/content/2006-01-0316/`.

[15] Gulshan Noorsumar, Svitlana Rogovchenko, Kjell G. Robbersmyr, Dmitry Vysochinskiy, and Andreas Klausen. A novel technique for modeling vehicle crash using lumped parameter models. *Proceedings of the 11th International Conference on Simulation and Modeling Methodologies, Technologies and Applications, SIMULTECH 2021*, pages 62–70, 2021. doi: 10.5220/0010529200620070.

[16] National Highway Traffic Safety Administration et al. Crash simulation vehicle models. *URL: https://www. nhtsa. gov/research-data/databasesand-software*, 2016.

[17] Harry Singh, Velayudham Ganesan, James Davies, Mahendran Paramasuwom, Lorenz Gradischnig, Patrick Wood, and Vikrant Mogal. Structural countermeasure/research program mass and cost increase due to oblique offset moving deformable barrier impact test. Technical report, 2018.

[18] D Marzougui, D Brown, H K Park, C D Kan, and K S Opiela. Development & Validation of a Finite Element Model for a Mid-Sized Passenger Sedan. In *3 th International LS-DYNA Users Conference Session: Automotive*, 2014.

[19] Center for Collision Safety and Analysis – 2010 Toyota Yaris. URL `https://www.ccsa.gmu.edu/models/2010-toyota-yaris/`.

[20] Matthew Huang. *Vehicle crash mechanics*. CRC press, 2002.

[21] Javad Marzbanrad and Mostafa Pahlavani. A system identification algorithm for vehicle lumped parameter model in crash analysis. *International Journal of Modeling and Optimization*, 1(2):163, 2011.

[22] Witold Pawlus, Hamid Reza Karimi, and Kjell Gunnar Robbersmyr. Development of lumped-parameter mathematical models for a vehicle localized impact. *Journal of mechanical science and technology*, 25(7):1737–1747, 2011.

[23] Bernard B Munyazikwiye, Dmitry Vysochinskiy, Mikhail Khadyko, and Kjell G Robbersmyr. Prediction of vehicle crashworthiness parameters using piecewise lumped parameters and finite element models. *Designs*, 2(4):43, 2018.

[24] Bernard B Munyazikwiye, Hamid R Karimi, and Kjell G Robbersmyr. Application of genetic algorithm on parameter optimization of three vehicle crash scenarios. *IFAC-PapersOnLine*, 50(1):3697–3701, 2017.

[25] Andreas Klausen, Sondre Sanden Tørdal, Hamid Reza Karimi, Kjell G Robbersmyr, Mladen Ječmenica, and Ole Melteig. Mathematical modeling and optimization of a vehicle crash test based on a single-mass. In *Proceeding of the 11th World Congress on Intelligent Control and Automation*, pages 3588–3593. IEEE, 2014.

[26] Gulshan Noorsumar, Kjell Robbersmyr, Svitlana Rogovchenko, and Dmitry Vysochinskiy. Crash Response of a Repaired Vehicle - Influence of Welding UHSS Members. In *WCX SAE World Congress Experience*. SAE International, 4 2020. doi: https://doi.org/10.4271/2020-01-0197. URL `https://doi.org/10.4271/2020-01-0197`.

[27] Herbert Goldstein, Charles Poole, John Safko, and Stephen R. Addison. Classical Mechanics, 3rd ed. *American Journal of Physics*, 70(7):782–783, 7 2002. ISSN 0002-9505. doi: 10.1119/1.1484149. URL `http://aapt.scitation.org/doi/10.1119/1.1484149`.

[28] Sergio M Savaresi, Charles Poussot-Vassal, Cristiano Spelta, Olivier Sename, and Luc Dugard. *Semi-active suspension control design for vehicles*. Elsevier, 2010.